

Allyl Alcohol Production by Conversion of Glycerol Over Supported Iron and Nickel Bimetallic Oxides

Nancy Martín^{1*}, María de Lourdes Rodríguez¹, Dora Solís-Casados², Margarita Viniegra¹

¹Dept. Química. Universidad Autónoma Metropolitana-Iztapalapa, Av. San Rafael Atlixco N° 186. 09340 CDMX, México.

²Universidad Autónoma del Estado de México. Centro Conjunto de Investigación en Química Sustentable UAEM-UNAM, Toluca, Edo. de México. México.

*Corresponding author: Nancy Martín, email: mgnc@xanum.uam.mx, Phone number: 52 55 5804 4600 (x4317).

Received July 1st, 2020; Accepted September 24th, 2020.

DOI: <http://dx.doi.org/10.29356/jmcs.v64i4.1246>

Abstract. The study of catalysts based on iron, nickel, and iron-nickel oxides (Fe, Ni and FeNi) supported on a commercial mesoporous alumina is presented. The metal oxides were synthesized by the incipient wetness impregnation method. The samples were characterized by XRD, H₂-TPR, Raman spectroscopy, XPS and N₂ adsorption. The catalytic activity was evaluated in the dehydration-dehydrogenation reaction of glycerol in the gas phase. In the iron oxide and nickel oxide catalysts, the result of H₂-TPR showed that the presence of nickel influences the reduction of iron species. In the reaction, the catalysts showed similar conversion. However, the selectivity of the bimetallic oxide catalysts is modified, and the production of allyl alcohol increases noticeably forming a greater amount allyl alcohol than that observed in the monometallic oxides, in which a greater amount of hydroxyacetone is formed. The results indicate that the redox pairs Fe⁺³/Fe⁺² influence the selectivity of these oxides. A decrease in the ratio Fe⁺³/Fe⁺² species favored the formation of allyl alcohol.

Keywords: Iron oxides; glycerol; magnetite; hematite; allyl alcohol; Fe_xO_y-NiO.

Resumen. Se presenta el estudio de catalizadores basados en óxidos de hierro y níquel (Fe, Ni y FeNi) soportados en una alúmina mesoporosa comercial. Los óxidos metálicos se sintetizaron por el método de impregnación de humedad incipiente. Las muestras se caracterizaron por XRD, TPR-H₂, espectroscopía Raman, XPS y adsorción de N₂. La actividad catalítica se evaluó en la reacción de deshidratación-deshidrogenación de glicerol en la fase gaseosa. En los catalizadores de óxido de hierro y óxido de níquel, el resultado de TPR-H₂ mostró que la presencia de níquel influye en la reducción de las especies de hierro. En la reacción, los catalizadores mostraron una conversión similar. Sin embargo, la selectividad en los catalizadores de óxidos bimetallicos se modifica formando una mayor cantidad de alcohol alílico que la observada en los óxidos monometálicos, donde se forma una mayor cantidad de hidroxiacetona. Los resultados obtenidos indican que los pares redox Fe⁺²/Fe⁺³ influyen en el comportamiento catalítico de estos óxidos, en la selectividad. Una disminución de la relación Fe⁺³/Fe⁺² favorece la formación de alcohol alílico.

Palabras clave: Óxidos de hierro; glicerol; magnetita; hematita; alcohol alílico; Fe_xO_y-NiO.

Introduction

Iron is known to be an active catalyst and a promoter in several catalytic reactions, such as the Fisher-Tropsch synthesis [1], the oxidation of CO [2], Fenton-type reactions [3] and the water gas shift reaction [4]. Among the attractive properties of the iron-based catalysts are their activity, low cost, and redox properties.

It is known that iron can be present in different forms, such as isolated $\text{Fe}^{+3}/\text{Fe}^{+2}$ species, various forms of oxides, hydroxides or oxyhydroxides [5] and the identification of each one of them by a technique is not easy. In addition, through the thermal treatments a specific iron material can undergo changes that are not always visible. In the same way, during the reaction, intermediates with hydroxide groups can be formed that may affect the acidity of the catalytic surface and, consequently, modify the selectivity of the reaction mixture [6].

The glycerol, produced as a by-product in the soap and biodiesel industries, into more valuable chemicals such as acrolein, hydroxyacetone, 1,2 and 1,3-propanediol and esters, has been a matter of increased interest in the last decade.

F. Delgado et al. reported [7] that iron-based supported catalysts are active in the glycerol gas phase reaction producing a high proportion of acrolein. They also showed that nickel can influence the selectivity of iron catalysts improving the catalytic activity and modifying the selectivity. Nickel is also very active for oxidation and hydrogenation reactions since it adsorbs both oxygen and hydrogen under certain conditions. In addition, it can serve as a seed for a better dispersion of iron inducing a modification of the active surface [7]. For example, in the methane reforming reaction, the bimetallic NiFe catalyst turned out to be a more active catalyst than monometallic Ni, due to the stabilization of the metals in the bimetallic particles [4].

On the other hand, in the reductive amination of isopropanol it was observed that in NiFe / γ - Al_2O_3 catalysts the nickel reducibility was affected by the iron species and, thus, the catalytic activity [8].

With respect the transformation of glycerol, De Oliveira et al. [9] studied the dehydration reaction of this compound with acid catalysts, such as zeolite β and zeolite Y. They obtained mostly acrolein, and hydroxyacetone (acetol) in very small quantities. In this context, it is well known that the conversion and selectivity to acrolein or to hydroxyacetone is very dependent not only on the number and nature of the acid sites but also on the textural properties of the catalysts [10,11]. However, the major disadvantage of the vapor-phase dehydration of glycerol to acrolein over acidic solid catalysts is carbon deposits [9]. To reduce carbon deposition, the addition of noble metals has been proposed. In this sense, Pd-HPW/Zr-MCM-21 showed higher acrolein selectivity, lower carbon deposition and higher stability than the catalysts without addition of Pd [12].

The direct conversion of glycerol to allyl alcohol is a less studied reaction. The allyl alcohol is an important chemical intermediate since it is very reactive due to presence of C=C and O-H functionalities. Allyl alcohol derivatives can be found in the cosmetic, pharmaceutical and food industries and are also raw materials for a wide variety of chemical products.

The production of allyl alcohol mainly involves the conversion of propylene; however, it can be obtained in a one-pot reaction from glycerol. This reaction can be achieved over iron catalysts in a two-step process: acrolein formation followed by the selective hydrogenation of the double bond in acrolein promoted by glycerol or other alcohols [6,13,16,25]. Catalysts such as zirconia-iron [13], MoO_3 - WO_3 / TiO_2 [14], and vanadium supported zeolite beta [15] have been found to selectively catalyze the formation of allyl alcohol from glycerol. Sanchez G et al. [16] used ZSM-5 and alumina supported iron catalysts to promote the formation of allyl alcohol, and they found a correlation between the acid or basic sites concentration and the allyl alcohol selectivity, but the role of iron was no clear. It has been proposed that the iron species promote the formation of allyl alcohol through a hydrogen transfer reaction that may involve chemical intermediates from the dehydration of glycerol [15].

In reducible materials the changes in the oxidation state of the metallic species have an important effect on the acidic properties of the catalyst which in turn influences the deposition of surface carbon residues and, thus, the stability of the catalyst [10,15]. In reducible materials, then, both the acidic and redox properties influence the activity and the selectivity in the dehydration of glycerol.

In this work we evaluate the ability of iron oxides ($\text{Fe}^{+2}/\text{Fe}^{+3}$ species), supported on a mesoporous alumina, and its modifications with nickel oxide, to produce allyl alcohol from the dehydration/dehydrogenation reactions of glycerol in the gas phase.

Experimental

Supported iron oxides and nickel oxides were prepared by the conventional incipient wetness impregnation method using a commercial mesoporous γ -alumina (Sigma-Aldrich) as support. $\text{Ni}(\text{NO}_3)_2 \cdot 6\text{H}_2\text{O}$ and $\text{Fe}(\text{NO}_3)_3 \cdot 9\text{H}_2\text{O}$ were used as precursor salts (both from Sigma-Aldrich). For the monometallic oxide catalysts, the nickel or the iron loading was fixed at 3.8×10^{-3} metal molar concentration (5 wt % metal loading) for 2 g of catalyst. The support was stirred with the required amount of an aqueous solution of the precursor salt at room temperature for 2 h. These samples were denoted as (Fe/A) and (Ni/A). For the series of bimetallic oxides, three catalysts were prepared with variable Fe/Ni molar ratio: 1/1 (FeNi/A), 0.2/0.8 (Fe_1Ni_4) and 0.8/0.2 (Fe_4Ni_1). Then, the catalysts were dried at 100 °C overnight and calcined in air for 4 h at 400 °C.

The samples were characterized by N_2 adsorption-desorption isotherms (BET analysis), X-ray diffraction (XRD), Raman spectroscopy, X-ray photoelectron spectroscopy (XPS), temperature-programmed reduction with hydrogen (H_2 -TPR) and FTIR spectroscopy of adsorbed pyridine.

The Brunauer-Emmett-Teller (BET) specific surface area, average pore diameter and pore volume were measured by a Quantachrome Autosorb-3B equipment using the nitrogen adsorption method. Prior to the measurements all samples were evacuated at 200 °C for 4 h at a pressure of 1.0×10^{-3} kPa to ensure complete removal of adsorbed moisture.

For the X-ray diffraction (XRD) experiments an X-ray diffractometer (Siemens) was used with $\text{CuK}\alpha$ radiation.

All Raman spectra were recorded at room temperature with a Horiba Jobin-Yvon Lab Ram HR 800 micro-Raman system, equipped with an Olympus BX40 confocal microscope (Edison, NJ, USA) and a CCD detector (Edison, NJ, USA). Measurements were performed using an excitation wavelength of 532.1 nm, a $50 \times$ objective, at a power close to 7 mW on the sample and 100 accumulations of 20 s per spectrum to improve the signal-to-noise (S/N) ratio. The spectra were calibrated using the 521 cm^{-1} line of monocrystalline silicon.

H_2 -TPR profiles were obtained by using an Altamira Instruments AMI-90; the samples (about 0.100 g) were pre-treated at 500 °C for 2 h under flowing nitrogen. A mixture of 10 %v/v H_2/Ar (50 mL/min) and a 2°C/min temperature ramp started from ambient temperature up to 900 °C, were used.

Pyridine (Py) adsorption was followed by FTIR measurements with a BELCAT-B FTIR spectrometer (BEL Japan Inc.) using a home-made quartz cell, allowing sample vacuum ($\approx 10^{-5}$ Torr) and temperature pretreatment (400 °C, 1 h). Py was adsorbed on the sample at its vapor pressure in flowing nitrogen at 150 °C for 30 min. Desorption data were collected at ambient temperature, 320 °C and 400 °C. Spectral bands at 1545 cm^{-1} (Brønsted sites) and 1450 cm^{-1} (Lewis sites) were considered for the estimation of acid sites concentration, using the molar extinction coefficients of $2.22 \text{ cm}^2/\mu\text{mol}$ (Lewis) and $1.67 \text{ cm}^2/\mu\text{mol}$ (Brønsted) [17].

XPS wide and narrow spectra were obtained with a JPS-9200 spectrometer from JEOL with a monochromatic Al $\text{K}\alpha$ X-ray source (energy=1486.68 eV). In each elemental region, charge shift was adjusted using the binding energy of carbon (1s) peak centered at 285 eV and used as internal standard to compensate for charge effects. Before the measurements, all samples were evacuated at ambient temperature for 8-10 h at a pressure of 1.0×10^{-6} Torr. Each acquired spectrum were processed deconvoluting the peaks inside it.

The catalysts were evaluated in the reaction of glycerol in the gas phase at atmospheric pressure and temperature of 300 °C, using about 0.100 g of catalysts in a vertical fixed-bed reactor. Before each test, the catalyst was maintained for 1 h at 400 °C under a flux of nitrogen. The evaporator feed solution was 20% w/w glycerol-water, which was supplied by means of a piston pump with a rate of $3 \text{ mL} \cdot \text{h}^{-1}$. The carrier gas was nitrogen at a flow rate $15 \text{ mL} \cdot \text{min}^{-1}$. The reaction products were collected with a condenser under water and ice at 0 °C. The reaction mixture was sampled every hour and analyzed in a Perkin-Elmer Clarus580 gas chromatograph equipped with a flame ionization detector and a capillary column Elite-Wax (30mx0.45 mm). For these analyses the split ratio was 100:1. The injector temperature was 250 °C, detector temperature 300 °C, oven initial temperature 35 °C (for 5 min) and then heated at rate of 10 °C/min to 200 °C and holding this temperature for 20 min. For quantitative measurements cyclohexanone was used as the internal standard. The reaction was carried out at a gas hourly space velocity (GHSV) of glycerol of 9 h^{-1} . The GHSV was defined as the volume flow rate of vaporized glycerol at 300 °C and 101.325 kPa divided by volume of catalyst (ca. 1 mL). The molar rate at three hours of reaction (r) was calculated using the molar flow ratio, mass of the catalyst and

the molar conversion of glycerol. The conversion of glycerol (%C) and the molar selectivity (%S), were calculated as follows:

$$\text{Glycerol conversion (\%C)} = [(\text{reacted moles glycerol})/(\text{moles glycerol in feed})]*100$$

$$\text{Product Selectivity (\%S}_i) = [(\text{formed moles product } i)/(\text{consumed moles glycerol})]*100$$

Results and discussion

The textural properties of the samples are shown in Table 1. No noticeable changes were observed in the textural properties of the Fe/A and Ni/A catalysts respect to the commercial support (A) therefore, the mesoporous structure is maintained. The N₂-isotherm obtained from the γ -Al₂O₃ (not shown) is a type IV isotherm with a H2 hysteresis loop, indicating that calcined support exhibited mesoporous structure [8]. The specific surface area (S_{BET}) changes slightly, the pore diameters (D_p) and the pore volumes (V_p) decreases in the bimetallic oxides when the metals are incorporated to the support, which suggests that the impregnation of the nickel or iron species presumably blocks some pores of the alumina.

Table 1. Textural properties of samples.

Samples	Pore* size/nm	Surface Área/m ² /g
A	34.5	101.7
Fe/A	30.3	112.1
Ni/A	30.2	94.4
FeNi/A	21.9	115.3
Fe ₁ Ni ₄ /A	17.7	112.9
Fe ₄ Ni ₁ /A	17.5	113.9

*Calculated by BJH method

The X-ray diffraction patterns (XRD) of the calcined catalysts in the mid-angle range are given in Fig. 1. The broadening of the XRD reflections indicates that the particle size of the catalysts is very small. Typical reflections of alumina (γ -Al₂O₃) are observed (JCPDS 79-1558), in $2\theta \approx 37.5^\circ$, 45.7° and 66.7° [5]. The peaks at $2\theta \approx 32^\circ$ and 38° are assigned to the hematite phase of Fe₂O₃ as well as those of iron oxides (γ -Fe₂O₃ and Fe₃O₄) (JCPDS 89-0597 and 88-0315). Reflections at $2\theta \approx 44^\circ$ can be of a nickel oxide (NiO) phase (JCPDS 47-1049) interacting with iron species, the peaks of which overlap with those of alumina. No metallic Ni diffraction peaks are observed. The crystallite size of alumina was determined by the Scherrer equation [5], and the diffraction peak of alumina at $66.7^\circ 2\theta$. No significant differences were observed in the values found (55 and 48 Å). So, the diffraction peaks and the crystallite size of the alumina phase in all samples suggest that the crystalline properties of the alumina are not affected by the metals.

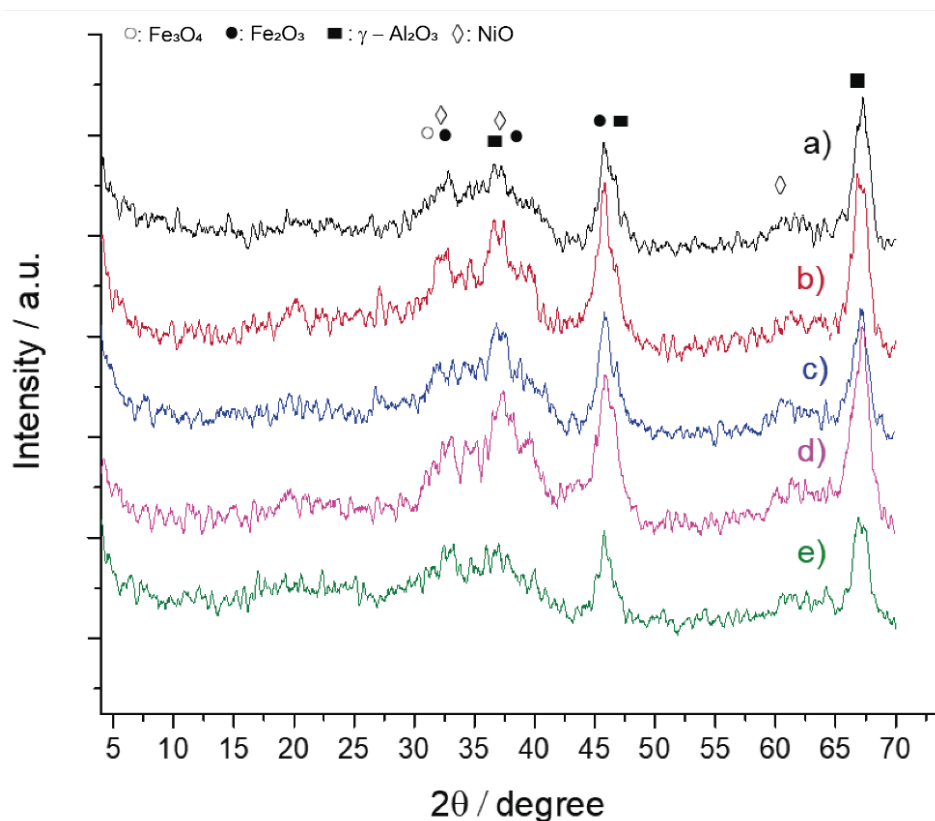


Fig. 1. Diffractograms DRX of samples: a) Fe/A; b) Ni/A; c) FeNi/A; d) Fe₁Ni₄/A; e) Fe₄Ni₁/A.

The Raman spectra of the bimetallic oxide samples are shown in the Fig. 2. The figure shows distinct phases of iron oxide that are present in the samples, such as hematite (Fe₂O₃), magnetite (Fe₃O₄) and maghemite (γ-Fe₂O₃) as well as nickel oxide (NiO). The vibrational modes of magnetite, hematite and maghemite structures in Raman spectroscopy are summarized in Table 2. Some of the reported magnetite bands [18,19] are close to the values expected for hematite. These bands (350, 500 and 700 cm⁻¹) are not well defined and a variation in its intensity is observed between the bimetallic samples depending if the oxides contain Fe⁺² or Fe⁺³. The differences observed in the intensities of the peaks between monometallic and bimetallic oxides can be due to the lower content of iron in the bimetallic oxides and to the surface morphology of the catalysts. For FeNi/A the strong band at 700 cm⁻¹ suggests a greater presence of Fe₃O₄ in this catalyst. However, it is difficult to distinguish the oxidation state of these oxides since their crystallinity is low.

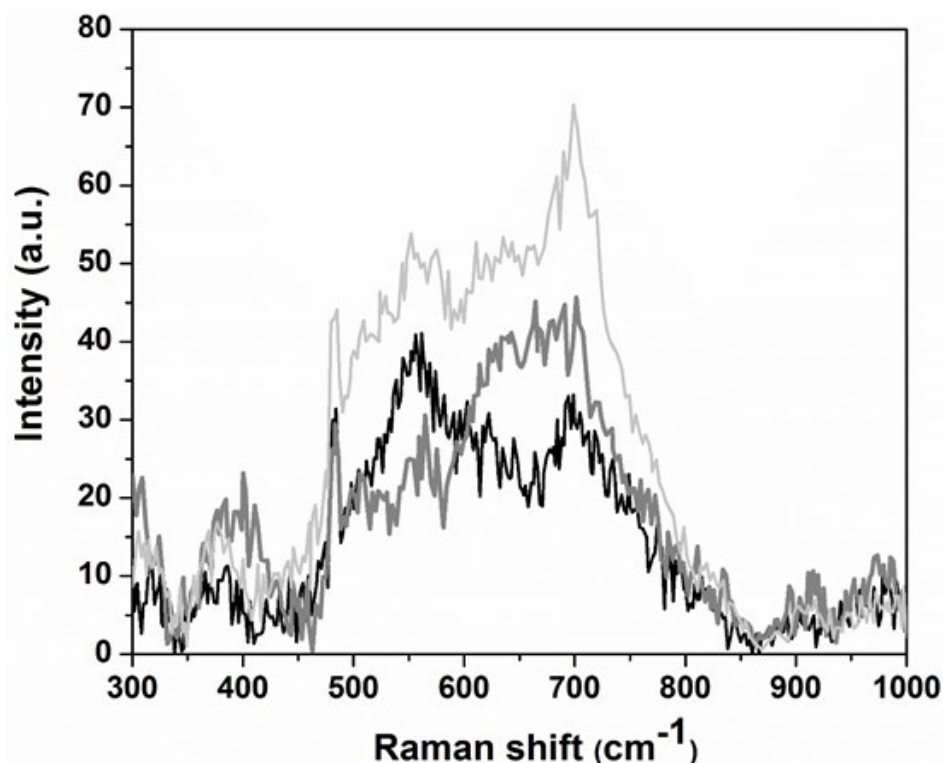


Fig. 2. Raman spectrum of bimetallic oxide samples: (-) $\text{Ni}_4\text{Fe}_1/\text{A}$; (-) $\text{Ni}_1\text{Fe}_4/\text{A}$; (-) NiFe/A .

Table 2. Wavenumbers (ν) observed in the Raman spectrum of bimetallic samples.

ν (cm^{-1})		Structural	
$\text{Fe}_1\text{Ni}_4/\text{A}$	FeNi/A	$\text{Fe}_4\text{Ni}_1/\text{A}$	Observations
300	303	300	magnetite
384	369	400	nickel oxide
484	483	483	hematite
556	552	564	magnetite
694	698	701	magnetite or maghemite
978	958	970	nickel oxide
1045	1031	1039	nickel oxide or maghemite

It has also been reported [18] that the oxyhydroxides ($\delta\text{-FeOOH}$, 300 cm^{-1} y 483 cm^{-1}) can show the characteristic peaks of hematite. Moreover, it is known that the Raman spectrum of FeO is very similar to that Fe_3O_4 [18], nevertheless FeO decomposes into magnetite under illumination. Transformation of magnetite, or maghemite, into hematite is a very common phenomenon in nature [5,18,19]. Still, analyzing the characteristic peaks of each sample, the Raman spectrum indicates a mixture of various phases and the proportions between them fluctuate along the series. For nickel there are two bands characteristic of NiO at *ca.* 400 cm^{-1} and 960 cm^{-1} [23].

To analyze the reducibility and the metal-support interactions, H₂-TPR experiments were performed and the results are shown in the Fig. 3.

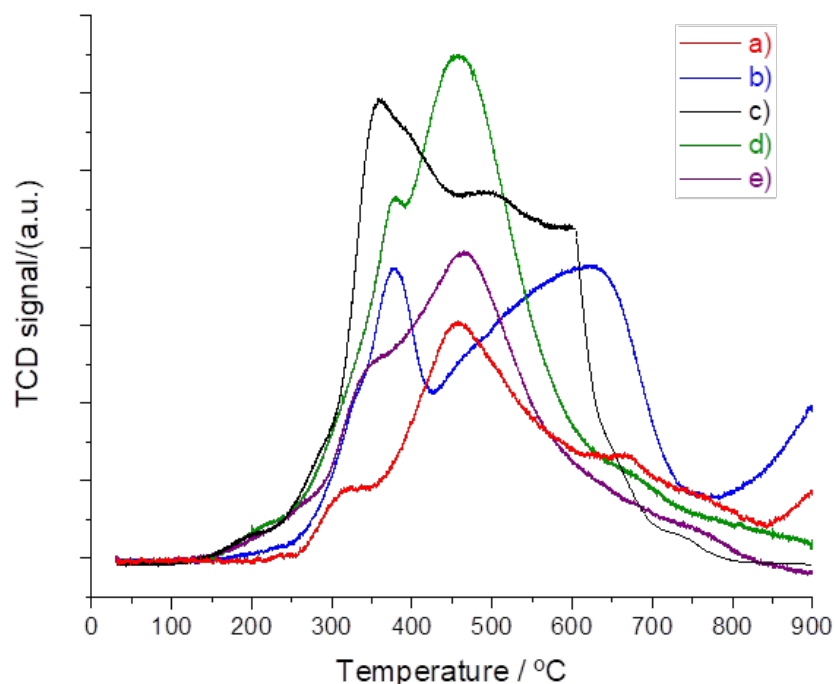


Fig. 3. H₂-TPR of samples: a) Ni/A; b) Fe/A; c) FeNi/A; d) Fe₄Ni₁/A; e) Fe₁Ni₄/A.

The H₂-TPR profile of the catalysts can be divided into three main regions (i.e., α , β , γ , peaks, in Table 3): the first centered in the region of lowest temperature (peak α) at ≈ 300 - 375 °C, the second one (peak β) located at ≈ 450 - 575 °C and the third (peak γ) centered at temperatures greater than 700 °C.

Table 3. Evolved peak temperatures obtained from H₂-TPR profiles.

CATALYSTS	T/°C		
	Peak α	Peak β	Peak γ
Ni/A	325	450	>700
Fe/A	375	625	>700
Fe ₁ Ni ₄ /A	325	475	---
FeNi/A	350	525	---
Fe ₄ Ni ₁ /A	375	450	---

The profiles of the monometallic oxide catalysts, Ni/A and Fe/A, show two hydrogen consumption peaks in the region α and β , due to the reduction of NiO species ($\text{Ni}^{+2} \rightarrow \text{Ni}^0$) that do not interact with the support, and to the reduction of iron oxide species –first Fe₂O₃ and then Fe₃O₄ to FeO [22]. Furthermore, the peak that starts at temperatures greater than 700 °C (peak γ), can be attributed to the reduction of FeO to Fe [6, 22] and to the reduction of NiAl₂O₄ spinels [23].

Both Ni and Fe suffer modifications of their reduction behavior when they are in combination with the second metal oxide. One of these is the high temperature region in the bimetallic catalysts; it can be observed that there is no consumption of hydrogen indicating that the Ni species that are strongly interacting with the support are either not present on the bimetallic samples or are reduced at much lower or much higher temperatures. In a similar manner one can think that the reduction of FeO to Fe is either proceeding at a lower temperature or at a much higher one, but since no metallic iron was observed in the XRD patterns, it has to be concluded that the reduction of FeO occurs at temperatures greater than 700 °C.

On the other hand, the low temperature profile of the bimetallic oxides catalysts is very different from that of the monometallic ones. The first reduction peak (α) of the Ni/A catalysts appears at 325 °C and in the other samples this peak is present at either 325°C or at a higher temperature. In the bimetallic oxides the second reduction peak (β) of FeNi/A is very different from the other samples. The reduction processes in the bimetallic samples begin 100 degrees before the reduction processes of Fe/A. This implies that the presence of nickel oxide favors the reduction processes of iron species in the bimetallic oxide samples and this may be an important factor to consider in the catalytic activity of these solids. Such a profile modification in the bimetallic samples may be due to an interaction between the two oxides and this may produce active redox pairs.

Fig. 4 shows the Fe 2p XPS spectra of Fe/A, where three doublets were observed (and the corresponding satellite peaks) with binding energies for the first doublet peaking close to 706 and 715 eV, the second doublet with peaks close to 710 and 719 eV and the third doublet with peaks at 712 and 722 eV, which were attributed to Fe, Fe⁺² and Fe⁺³, respectively [20].

For the bimetallic oxides, the Fe 2p peaks were shifted to higher binding energies, and this may be explained by an enhanced electron density of the Fe species due to the presence of nickel (Table 4) [3, 22]. In the Ni 2p XPS spectra (not showed), even when a lot of noise was observed and, also, low intensities, two peaks located at \approx 855 and 871.6 eV were detected, corresponding to Ni⁺² from NiO and Ni⁺² peaks at 857 and 873.4 eV from NiAl₂O₄ spinel structure [23].

From the spectra, the relative amounts of the iron species in the monometallic and the bimetallic oxides were obtained. These results are shown in table 4. The data indicate that iron species including Fe, Fe₂O₃ and Fe₃O₄ coexisted in all samples. The first two species are in greater proportion in Fe/A sample, while in the bimetallic oxides this proportion changes.

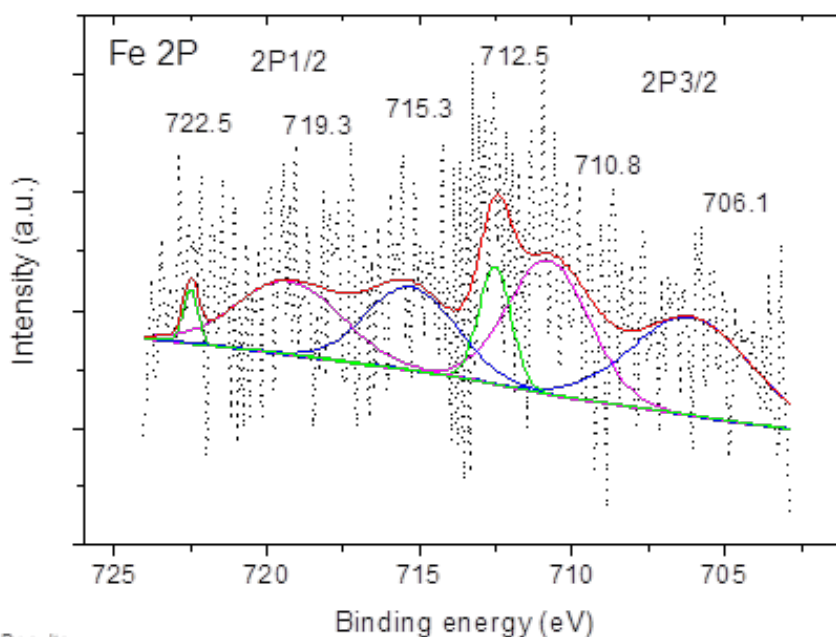


Fig. 4. XPS spectra of Fe/A.

Table 4. Binding energy (BE) and percentage composition of the XPS spectra.

Catalysts	First double BE (eV)		Second double BE (eV)		Third double BE (eV)		Fe ³⁺ /Fe ²⁺
	Fe	(Fe 2p)	Fe ₂ O ₃	(Fe 2p _{3/2})	Fe ₃ O ₄	(Fe 2p _{1/2})	
Fe/A	706.1	715.3	710.8	719.3	712.5	722.5	
%	44.47		44.69		10.84		4.12
Fe ₁ Ni ₄ /A	714.1	722.1	717.37	725.15	719.47	727.47	
%	43.32		39.33		17.33		2.27
FeNi/A	711.3	728.3	715.7	730.4	718.7	734.6	
%	31.44		34.46		34.07		1.01
Fe ₄ Ni ₁ /A	711.8	717.6	713.9	724.7	721.7	727.6	
%	29.75		36.43		33.78		1.08

The results for the bimetallic oxides show that although the presence of Ni can promote the reduction of the iron species, these remained mostly in their oxide forms, i. e., Fe₂O₃, Fe₃O₄, FeO and NiO as confirmed by Raman analyses and H₂-TPR measurements.

According to the literature [10,11,22] in bimetallic oxides NiFe catalysts, the reduction temperature of nickel is displaced to lower values by an interaction with the iron species. In addition, the metals species may also interact with the alumina support. However, the reduction of iron oxides at lower temperature in the NiFe/A may suggest that the addition of nickel oxide promotes the reduction of iron oxide particles, as reported in [23]. Nevertheless, in our samples the presence of iron oxide species was confirmed through Raman, XPS, and the H₂-TPR analyses. By XPS, the monometallic catalyst Fe/A showed a higher ratio Fe³⁺/Fe²⁺ pairs than the bimetallic oxide catalysts.

The acidic properties of the samples were measured by pyridine adsorption taking into consideration the bands at approximately 1550, 1480 and 1450 cm⁻¹ attributed to Lewis acid sites and the bands at 1530 and 1645 cm⁻¹ attributed to Brønsted acid sites [24]. In all the samples the bands disappear at 400 °C, i.e., high-strength acid sites are not present. In table 5, the concentrations of Lewis and Brønsted sites acid measured with the desorption of Py at 320 °C are shown. The amount of Brønsted acid sites on Fe/A and Fe₁Ni₄/A are higher than in the other samples. But there is no trend of the medium strength acidity (320°C) within the various catalysts, except for the Brønsted molar fraction which increases with the nickel content in the bimetallic samples. Nevertheless, it is evident that the addition of nickel impacts the acid properties of the catalysts, altering the concentration of the acid sites (C_B/(C_B+C_L)) by possible structural changes of the bimetallic oxides.

Table 5. Concentration of acid sites, Lewis (C_L) and Brønsted (C_B), by desorption of Py at 320 °C.

Catalysts	Fe/A	Fe ₄ Ni ₁ /A	FeNi/A	Fe ₁ Ni ₄ /A
C _L (μmol/g)	18.02	347.22	39.41	178.33
C _B (μmol/g)	152.7	38.92	4.99	170.67
C _B /(C _B +C _L)	0.89	0.10	0.11	0.49

The catalysts were evaluated in the transformation of glycerol in the gas phase. The conversion (%C), rate (r) and the molar selectivity (%S) values were obtained at 3.0 h of reaction, WHSV: 9 h⁻¹ and 300 °C and are shown in Table 6. It is observed that Ni/A is more active than Fe/A. While in the bimetallic oxides there are differences between them observing a lower activity in the FeNi/A. However, under similar reaction conditions (340°C, WHSV: 3 h⁻¹; 30 wt % glycerol) the value obtained in our work (ca. 90% C) is in agreement with that reported for a γ-Al₂O₃/Fe/Rb catalyst (90 % C) [25].

Under our reaction conditions the main products were acrolein (AC), allyl alcohol (AA), hydroxyacetone (HA), and other liquid and gaseous compounds that were not identified. However, the molar selectivity (%) that we report is normalized. As regards to the selectivity, notable differences are observed between the monometallic oxide and the bimetallic oxide catalysts.

Table 6. Rates (*r*) and molar Selectivities (%S) over the glycerol reaction. AA: allyl alcohol; AC: acrolein; HA: hydroxyacetone. (Reaction conditions: T: 300 °C, P: 1 atm; *t_R*: 3 h).

Catalysts	$r \times 10^4$	%S		
	molGlyc/s.g	AA	AC	HA
Fe/A	2.97	0	13.62	86.38
Fe ₄ Ni ₁ /A	3.07	63.46	5.12	31.42
FeNi/A	2.92	90.97	9.03	0
Fe ₁ Ni ₄ /A	3.16	0	12.20	87.80
Ni/A	3.120	0	17.71	82.29

The Ni/A, Fe/A and Fe₁Ni₄/A samples produce higher amounts of hydroxyacetone, while the bimetallic oxide catalysts with the greater amounts of iron, FeNi/A and Fe₄Ni₁/A, show an increase in the selectivity of allyl alcohol at the expense of hydroxyacetone. These two catalysts present the lowest molar fraction of Brønsted sites (Table 5), and the highest concentration of Fe²⁺ species (Table 4). These facts may point out the importance of redox sites in the selectivity of the bimetallic catalysts with lower amounts of nickel.

Lang et al [25] reported the effect of adding Fe-Mo species to KIT-6 silica. FeMo-KIT-6 bimetallic catalyst presented a much higher selectivity than the monometallic Mo-Kit-6. This is explained by a strong synergetic effect between Fe₂O₃ and MoO₃ which alters the surface, moderate acid strength, the number of acid sites and the reducibility of the surface species. Also, a synergetic effect was observed in Fe-Mo/HZSM-5 catalysts and FeO_x/NiO_y/SBA-15, the latter showing a positive contribution of the nickel species [3,26]. Therefore, it is clear that the allyl alcohol selectivity and glycerol conversion are strongly dependent on the acid-base and redox properties of the catalysts [10, 26].

Glycerol is a very reactive molecule due to the presence of primary and secondary hydroxyl groups that can be replaced by other functionalities. According to most of the literature [6] the dehydration reaction occurs mainly in the presence of acid sites, while in the presence of metals, hydrogenation or hydrogenolysis may occur due to the breakdown of C-O bonds or C-C bonds in the glycerol molecule.

The formation of allyl alcohol can happen by two stages; first, the dehydration of glycerol to form acrolein with the participation of acid sites, followed by another hydrogenation (redox sites or Lewis sites) to form allyl alcohol [15,27]. However, a hydrogen source is required to allow the dihydroxylation needed to obtain allyl alcohol. It should be mentioned that in both routes there is the formation of an enol intermediate, which could be determined by the ratio of the Brønsted/Lewis acid or redox sites involved in the reaction [6,10,21].

Martinuzzi et al. [21] and Liu et al. [6] relate acrolein and allyl alcohol formation to one synthesis route, while the formation of hydroxyacetone follows a different path. It is proposed that the Brønsted acid sites lead to acrolein production, while the Lewis acid or redox sites produces mainly hydroxyacetone by means of the enol intermediate [6,10]. The Fe_xO_y plays an important role in providing redox sites for this reaction. So, the pathway proposed by G. Sanchez et al. [16,27] for the allyl alcohol formation is consistent with our results for the bimetallic oxide samples, since its formation is attributed to a consecutive reaction in which the enol intermediate formed on the redox sites (Fe⁺³/Fe⁺² in this work), results in a higher selectivity to allyl alcohol (Fig. 5).

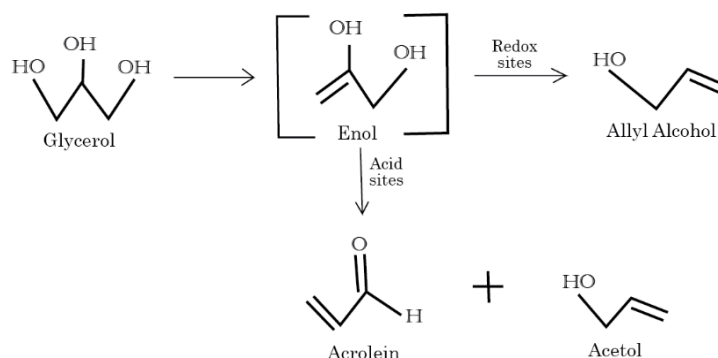


Fig. 5. Possible reaction pathways from glycerol to allyl alcohol.

The changes observed in the selectivity of our catalysts can be attributed to the presence of various ratios of $\text{Fe}^{+3}/\text{Fe}^{+2}$, obtained by XPS, Raman, and TPR- H_2 experiments, and supports the proposal to include the redox pairs in the reaction mechanism. This suggests that a decrease in the $\text{Fe}^{+3}/\text{Fe}^{+2}$ ratio favors the formation of allyl alcohol.

Conclusions

The textural properties of the support, obtained by nitrogen physisorption, did not show notable differences with the catalysts, indicating that the mesoporous nature of the support was not altered by the deposition of the metals.

The XRD diffractograms, XPS, and Raman spectra of the catalysts revealed the presence of nickel oxide (NiO) and iron oxide (Fe_3O_4 and Fe_2O_3) phases, i.e. the presence of $\text{Fe}^{+3}/\text{Fe}^{+2}$ pairs.

In the analysis of the reduction profiles (H_2 -TPR), it was observed that the reduction behavior of both Ni and Fe was altered by the presence of the second metal in the samples, reducing the temperature that initiates the reduction processes and modifying the reduction of the nickel aluminates and of FeO.

All the catalysts were found to have similar activities with notable differences in their selectivity. These differences are explained by the interaction between the metal oxides in the bimetallic catalysts, which produces changes in the $\text{Fe}^{+3}/\text{Fe}^{+2}$ ratio. The production of allyl alcohol on the bimetallic oxides may be explained by the redox properties of these catalysts. A decrease in the $\text{Fe}^{+3}/\text{Fe}^{+2}$ ratio, favors the formation of allyl alcohol.

Acknowledgemnts

The authors are grateful for financial support of UAM-I-CA-156 of PRODEP-SEP. We also thank to Dr. Michel Picquart (UAMI) for the Raman spectra of samples, Dra. Aída Gutiérrez (UNAM) for the experiments with pyridine adsorption and to Dra. Iris Serratos (UAMI) for the help in the elaboration of the figures.

References

1. Feyzi, M.; Mirzaei, A.A. *Petroleum Chemistry* **2012**, 5, 362-371. DOI: /10.113/S096554411205002.
2. Dreyer, J.A.H.; Grossmann, H.K.; Chen, J.; Greb, T.; Gong, B.B.; Sit, P.H.L.; Madler, L.; Teoh, L. *Y. J. of Cat.* **2015**, 329, 248-261. DOI:/10.1016/j.jcat2015.5.003.

3. Li, X.; Liv, W.; Ma, J.; Wen, Y.; Wu, Z. *Appl.Catal B.* **2015**, *179*, 239-248. DOI: /10.1016/apcatb.2015.05.034.
4. Margossian, T.; Larnier, K.; Kumeich, F.; Muller, C.; Coperet, C. *ACS Catalysis* **2017**, *7*, 6942-6948. DOI: /10.1021/acscatal.7b02091.
5. Lubbe, M.; Gigler, A.M.; Stark, R.W.; Moritz, W. *Surface Science* **2010**, *604*, 679-685. DOI: /10.1016/j.susc.2010.01.015.
6. Liu, Y.; Tuysuz, H.; Jia, Ch. J.; Schwickardi, M.; Rinaldi, M.; Lu, A.H.; Schmidt, W.; Shut, F. *Chem. Comm.* **2010**, *46*, 1238. DOI: /10.139/b921648k.
7. García-Delgado, F.J.; Viniegra, M.; Córdoba, G.; Martín, N. *Actas XXV CICAT* **2016**, P447, Montevideo, Uruguay.
8. Hong, E.; Bang, S.; Cho, J.H.; Jung, K.D.; Shin, C.H. *Appl. Catal. A.* **2017**, *542*, 146-153. DOI: /10.1016/j.apcata.2017.05.003.
9. De Oliveira, A.S.; Vasconcelos, S.T.; De Sousa, J.R.; Filho, J.M; Oliveira, A.E. *Chem. Eng. J.* **2011**, *168*, 765. DOI: /10.1016/j.cej.2020.09.029.
10. Santos, R.C.R.; Braga, D.M.V.; Pinheiro A.N.; Freire, V.N.; Longhinotti; Valentini A. *Catal. Sci. &Technology* **2016**, *6*, 4986-5002. DOI: /10.1039/c6cy0096g.
11. Martínez-Rico, M.; Aguilar-Pliego, J.; Pérez-Pariente, J.; Márquez, C.; Viniegra, M.; Martín, N. *RMIQ* **2018**, *17*, 523-532. DOI: /10.24275/uam/izt/dcbi/ revmexingquimica/ 2018v17n2/Martinez/.
12. Ma, T.L.; Yun, Z.; Xu, W.; Chen, L.G.; Li, L.; Ding, J.F.; Shan, R. *Chem. Eng. J.* **2016**, *294*, 343-352.
13. Yoshikawa, T.; Tago, T.; Nakamura, A.; Konaka, A.; Mukaida, M.; Masuda, T. *Res. Chem. Intermed.* **2011**, *37*, 1247-1256. DOI: /10.1007/s1164-011-0391-y.
14. Ulgen, A.; Hoelderich, W.F. *Applied Catalysis A: Gen.* **2011**, *400*, 34-38. DOI: 10.1016/j.apcata.2011.04.005.
15. Almeida, R.; Filipa Ribeiro, M.; Fernandes, A.; Lourenco, J.P. *Catalysis Communication* **2019**, *217*, 20-24. DOI: 10.1016/j.catcom.2019.04.015.
16. Sánchez, G.; Dlugogorski, B.Z.; Kennedy, E.M.; Stockenhuber, M.. *Applied Catalysis: A.* **2016**, *519*, 130-142. DOI: /10.1016/apcata.2015.09.039.
17. Emeis, C.A. *J. of Cat.* **1993**, *141*, 347-354. DOI: 0021.9517.
18. de Fairea, D.L.A.; Venancio Silva, S.; Oliveira, M.T. *J. of Raman Spectroscopy* **1997**, *28*, 873-878. DOI: CCC 0377-0486/97/110873-06.
19. Gerónimo-López, C.; Vázquez-Arenas, J.; Picquart, M.; González, I. *Electrochimica Acta* **2014**, *136*, 146-156. DOI: /10.1016/j.electacta.2014.05.069.
20. Wu, D.; Zhang, Y.; Wen, M.; Fang, H.; Wu, Q.. *Inorganic Chemistry* **2017**, 5152-5157. DOI: /10.1021/acs.inorg.chem.7b00304.
21. Martinuzzi, I.; Azizi, Y.; Davaux, J.F.; Tretjak, S.; Zahraa, O.; Leclerk, J.P. *Chem. Eng. Sci.* **2014**, *116*, 118-127. DOI: /10.1016/j.ces.2014.04.030.
22. Jin, Y.M.; Datsy, A.K. *J. of Cat.* **2000**, *196*, 8-17. DOI: /10.1006/jcat.2000.3024.
23. Tian, D.; Liu, Z.; Li, D.; Shi, H.; Pan, W.; Chang, Y. *Fuel.* **2013**, *104*, 224-229. DOI: /10.1016/j.fuel.2012.08.033.
24. Topaloglu-Yazici, D.; Bilgic, C. *Surf. Interface Anal.* **2010**, *42*, 959-962. DOI: /10.1002/sia.3474.
25. Lang, H.; Xiao, X.; Yuan, S.; Xhang, B.; Zhou, G.; Yiang, Y. *Catal. Letters* **2017**, *147*, 2187-2199. DOI:/10.107/s10562-017-2124-3
26. A. Kostyniuk, D. Bajec, P. Djinovic and B. Likozar. *Chem. Eng. Journal*, **2020**, *397*, 125430. DOI:/10.1016/j.cej.2020.125430.
27. G. Sánchez, J. Friggieri, C. Keast, M. Drewery, B.Z. Dlugogorski, E. Kennedy and M. Stockenhuber. *Appl. Catal. B.* **2014**, 152-153, 117-128. DOI:/10.1016/ j.apcatb.2014.01.019.